Complex Cation and Spin Orders in the High-Pressure Ferrite CoFe3O5

Complex cation and spin orders in the high pressure ferrite $CoFe_3O_5$

Ka H. Hong,[a] Elena Solana-Madruga,[a] Mauro Coduri,[b] and J. Paul Attfield*,[a]

[a]Centre for Science at Extreme Conditions and School of Chemistry, University of Edinburgh, West Mains Road, Edinburgh EH9 3FD, United Kingdom

[b]European Synchrotron Radiation Facility, 71 avenue des Martyrs, Grenoble, 38000, France

ABSTRACT: A ferrite in the $Sr_2Tl_2O_5$-type MFe_3O_5 family with M = Co has been synthesized at 12 GPa pressure. Neutron diffraction shows the sample to be Co-deficient with composition $Co_{0.6}Fe_{3.4}O_5$. The Co/Fe cation distribution is found to be profoundly different from those of MFe_3O_5 analogs and lies between normal and inverse limits as Co^{2+} substitutes across trigonal prismatic and one of the two octahedral sites. $CoFe_3O_5$ shows complex magnetic behavior with weak ferromagnetism below $T_{C1} \approx 300$ K and a second transition to ferrimagnetic order at $T_{C2} \approx 100$ K. Spin scattering of carriers leads a substantial increase in the hopping activation energy below T_{C1} and a small negative magnetoresistance is observed at low temperatures.

Introduction

Iron oxide spinels and related magnetic materials are important for many applications and also for fundamental interest in couplings between spin, charge, orbital and lattice degrees of freedom. Magnetite, Fe_3O_4, has been studied intensively since 1939 when Verwey reported a metal–insulator transition accompanied by a structural distortion.[1] The low temperature structure has a complex charge and orbital ordering that leads to the formation of trimerons – linear orbital molecule clusters of three Fe ions.[2] Further notable magnetic and electronic orders have subsequently been discovered in the underexplored Fe_nO_{n+1} and substituted $MFe_{n-1}O_{n+1}$ homologous series. The $n = 4$ phase Fe_4O_5, prepared using high pressure high temperature (HPHT) synthesis,[3] has an incommensurate charge order at 150 K below which dimeron and trimeron-like groups of Fe ions are formed,[4] and higher Fe_nO_{n+1} homologues with $n > 4$ have also been made at pressure.[5] Studies of $n = 6$ $CaFe_5O_7$ have revealed a coupled structural and magnetic transition at 360 K accompanied by charge ordering.[6,7,8]

In addition to Fe_4O_5, other $n = 4$ MFe_3O_5 phases have also been found to have notable properties. $CaFe_3O_5$ which was first reported in 1980 and can be prepared at ambient pressure,[9] has recently been shown to have long range electronic phase separation. Magnetic ordering below 302 K leads to segregation into Fe^{2+}/Fe^{3+} charge averaged and charge ordered phases with formation of trimerons in the latter.[10] $MnFe_3O_5$, discovered under HPHT conditions, shows a rich variety of magnetic ordered states on cooling below $T_N = 350$ K, and Fe^{2+}/Fe^{3+} charge ordering at 60 K leads to spin reorientation.[11,12] $MgFe_3O_5$ was also reported in a study of the Fe_4O_5 -$Mg_2Fe_2O_5$ solid solution, but the crystal structure and magnetic properties were not reported.[13]

The MFe_3O_5 phases adopt the orthorhombic $Sr_2Tl_2O_5$-type structure with space group *Cmcm*.[14] This has three independent cation sites M1, M2 and M3 in a 2:1:1 ratio, where M1 and M2 form edge-sharing MO_6 octahedra channeled by triangular prisms containing the M3 site, as shown in Figure 1. The M3 site is occupied by large M^{2+} = Ca, Mn and Fe cations in the above MFe_3O_5 materials. However it is unclear whether transition metals smaller than iron will also occupy trigonal prismatic M3 sites or will prefer octahedral M1 and M2. These alternative distributions are analogous to the much-studied normal and inverse cation arrangements in spinels. Hence we report here the HPHT synthesis of $CoFe_3O_5$, the crystal structure including the cation distribution, and the electrical and magnetic properties.
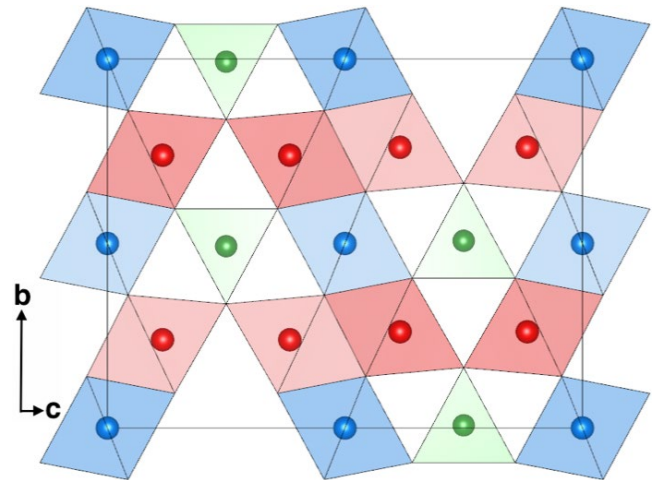
Figure 1. Polyhedral projection of the *Cmcm* structure of $CoFe_3O_5$ at 300 K with M1 site octahedra shown in red, M2 octahedra in blue and M3 triangular prisms in green. Oxygens are located at the corners of polyhedra.

Experimental Section

HPHT Synthesis. CoO and Fe_3O_4 powders were ground together in a 1:1 ratio, and were heated under pressure at 1200 °C in a Pt capsule for 20 min in a two-stage Walker-type module. Reaction at 10 GPa pressure was unsuccessful but 12 GPa gave a polycrystalline product of apparent composition $CoFe_3O_5$. Several batches of material were synthesized under the latter conditions.

Magnetic and Electrical Property Measurements. A Quantum Design MPMS XL SQUID magnetometer was used to carry out magnetization measurements. Electrical resistivity measurements were carried out with a Quantum Design PPMS.

Crystal and Magnetic Structures. HPHT reaction products were initially characterized by powder X-ray diffraction collected with a Bruker D2 diffractometer using Cu K$_\alpha$ radiation. High resolution powder synchrotron X-ray diffraction (PSXRD) data were collected at the ID22 beamline of the ESRF with incident wavelength 0.39994 Å. A glass capillary with an outer diameter of 0.3 mm was used to contain the polycrystalline sample of approximately 8 mg. Low temperature diffraction data were collected from 5 to 90 K using a liquid helium cryostat system and from 90 to 400 K with an Oxford Cryosystems nitrogen cryostream. High resolution time-of-flight powder neutron diffraction (PND) data were collected at the WISH beamline of the ISIS facility, with 50 mg of powder from several high-pressure syntheses packed into a vanadium can. Diffraction patterns were collected between 10 and 400 K using a closed cycle refrigerator (CCR) with a hot stage. The crystal and magnetic structures of CoFe$_3$O$_5$ were Rietveld-fitted using the FullProf Suite and General Structure Analysis System (GSAS),[15, 16] and images were generated using VESTA.[17]

Results and Discussion

Synthesis. Phase formation was confirmed using laboratory powder X-ray diffraction. A Rietveld fit to the diffraction pattern (Fig. S1) confirms an orthorhombic *Cmcm* phase isostructural with the MFe$_3$O$_5$ (M = Ca, Fe and Mn) analogs. The room temperature lattice parameters of CoFe$_3$O$_5$ are a = 2.8982(4), b = 9.767(2) and c = 12.567(1) Å, with a cell volume of V = 355.7(1) Å^3. Further structural results are described later.

Magnetic and Electrical Properties. Magnetic susceptibilities in Figure 2a reveal two magnetic transitions for CoFe$_3$O$_5$. A small magnetic upturn is observed at $T_{C1} \approx$ 300 K and a second transition is seen at $T_{C2} \approx$100 K. Both are accompanied by divergence of ZFC and FC measurements indicating ferromagnetic contributions. Magnetization-field loops shown in the inset of Figure 2 show a small remnant magnetization of M_r = 0.014 μ_B per formula unit at 350 K, mostly likely due to traces of ferromagnetic spinel impurities. M_r increases to 0.06 μ_B on cooling from 350 to 200 K through T_{C1}, revealing an intrinsic weak ferromagnetism, and increases further on cooling through T_{C2} to 0.75 μ_B at 2 K, consistent with a ferrimagnetic order. Two similar magnetic transitions were reported for MnFe$_3$O$_5$ at 350 and 60 K.[12]

The electrical resistivity of a polycrystalline pellet of CoFe$_3$O$_5$ shows semiconducting behavior (Figure 2b) and the resistance was too great to be measured below 120 K. The high temperature activation energy for electron hopping, fitted as an Arrhenius $\rho = A \exp(E_a/k_B T)$ dependence in Figure 2c, is E_a = 14 meV showing that the material behaves as a highly doped semiconductor. The slope deviates on cooling below $T_{C1} \approx$ 300 K (1000/$T_{C1} \approx$ 3.3) and the 130 to 245 K region has a substantially higher E_a = 112 meV revealing a strong antiferromagnetic spin scattering contribution. A small magnetoresistance effect of MR = -5% in a 7 T field at 125 K is observed, as shown in the inset to Figure 2b, consistent with partial suppression of the spin scattering term. CoFe$_3$O$_5$ has a larger - MR than CaFe$_3$O$_5$ due to a higher magnetization at low temperature.

(a)
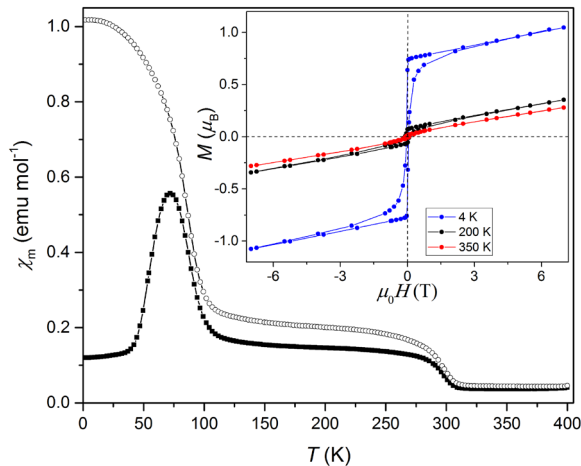
(b)
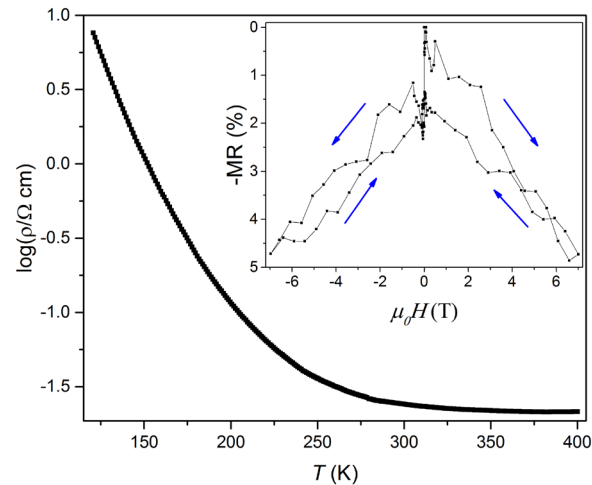
(c)
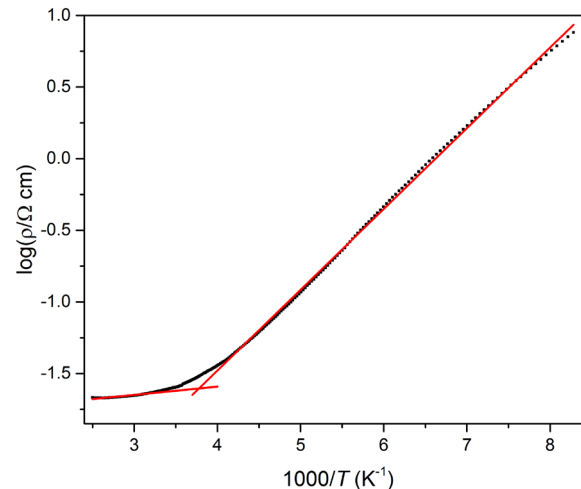
Figure 2. (a) Zero field cooled (ZFC, closed symbols) and field cooled (FC, open symbols) magnetic susceptibilities for CoFe$_3$O$_5$ in a 0.2 T field. Inset shows magnetization-field loops at 4, 200 and 350 K. (b) Log$_{10}$ of the electrical resistivity against temperature. Inset shows magnetoresistance at 125 K. (c) Log$_{10}$(resistivity)– reciprocal temperature plot showing Arrhenius fits above and below $T_{C1} \approx$ 300 K.

Crystal Structure Determination. The high contrast between the neutron scattering lengths of Fe and Co (9.45 and

2.49 fm respectively) enabled occupancies of the three cation sites to be determined from refinement against the high-resolution neutron diffraction data obtained at 400 K (Figure S2). This reveals that the M1 site is occupied exclusively by Fe while the M2 and M3 sites contain Fe/Co mixtures as shown in Table 1. The overall refined composition of $Co_{0.58}Fe_{3.42}O_5$ is Co-deficient. Refined amounts and compositions of CoO rock salt and $CoFe_2O_4$ spinel type secondary phases were 11.2(7)% $Co_{0.86}Fe_{0.14}O$ and 3.2(1)% $Co_{0.95}Fe_{2.05}O_4$, showing that these impurities are relatively Co rich. Further details are in Table S1. M-O bond distances and derived values for the Bond Valence Sum (BVS), estimated by a standard interpolation method,[18,19] are shown in Table 2.

Table 1. Lattice parameters, atomic coordinates, site occupancies and isotropic thermal displacements from neutron refinements in *Cmcm* space group of $CoFe_3O_5$ at 400 K (upper values) and 10 K (lower values). Estimated standard deviations in independent variables are shown in parentheses. χ^2 = 13.1 and 11.8, R_{wp} = 10.7 and 8.7%, and R_p = 12.9 and 10.1% at 400 and 10 K, respectively.

a /Å	b /Å	c /Å		Volume /Å³
2.9048(2)	9.7865(8)	12.5884(6)		357.86(4)
2.8836(1)	9.7968(3)	12.5385(5)		354.21(2)

Atom	x	y	z	Occ[a] Fe/Co	B_{iso} /Å²
M1	½	0.2438(6)	0.1166(3)	1/0	2.0(1)
		0.2419(5)	0.1176(3)		1.4(1)
M2	0	0	0	0.78(1)/ 0.22	2.0
					1.4
M3	0	0.4792(8)	¼	0.64(1)/ 0.36	2.0
		0.4834(8)			1.4
O1	½	0.3437(11)	¼	1	0.9(1)
		0.3460(11)			0.8(1)
O2	0	0.3569(7)	0.0447(6)	1	0.9
		0.3587(7)	0.0431(6)		0.8
O3	0	0.0902(8)	0.1449(6)	1	0.9
		0.0872(8)	0.1478(6)		0.8

[a] Variable occupancies were refined against 400 K neutron data and were fixed in lower temperature refinements.

The long average M3-O distance and the M3 BVS show that this trigonal prismatic site is occupied by divalent cations, in keeping with other $Sr_2Tl_2O_5$-type materials, while the similar average distances and BVSs for the octahedral M1 and M2 sites indicate that they have a mix of divalent and trivalent cations. The estimated Bond Valence Sums (BVSs) of the three cation sites in $CoFe_3O_5$ are similar to those of Fe_4O_5 at room temperature. The site-specific composition, written as

$(M3)(M1)_2(M2)O_5$ for comparison with the standard MFe_3O_5 formula, is thus $(Co^{2+}_{0.36}Fe^{2+}_{0.64})(Fe^{2+}_{0.33}Fe^{3+}_{0.67})_2(Co^{2+}_{0.22}Fe^{2+}_{0.11}Fe^{3+}_{0.67})O_5$ assuming that Fe is oxidized to the trivalent state in preference to Co. The cation distribution reveals that this Co-deficient sample lies between the postulated normal and inverse MFe_3O_5 distributions with around 60% of the substituted Co^{2+} at the trigonal prismatic sites (normal distribution), and the remaining 40% at the octahedral sites (inverse distribution).

Table 2. Metal-oxygen bond lengths with derived mean values < > and BVSs shown for $CoFe_3O_5$ at 400 K (upper values) and 10 K (lower values).

Bond	Distance (Å)	Bond	Distance (Å)
M1-O1	1.943(7)	M2-O2 (x 4)	2.095(6)
	1.948(7)		2.071(5)
M1-O2	2.257(9)	M2-O3 (x 2)	2.026(8)
	2.243(9)		2.040(8)
M1-O2 (x 2)	2.038(7)	<M2-O>	2.072(3)
	2.064(7)		2.061(3)
M1-O3 (x 2)	2.120(8)	BVS(M2)	2.4(1)
	2.127(7)		2.3(1)
<M1-O>	2.086(3)	M3-O1 (x 2)	1.967(9)
	2.096(3)		1.973(10)
BVS(M1)	2.4(1)	M3-O3 (x 4)	2.245(7)
	2.5(1)		2.180(7)
		<M3-O>	2.152(3)
			2.111(3)
		BVS(M3)	2.0(1)
			2.2(1)

A surprisingly strong preference for Co to substitute for Fe at the octahedral M2 but not the M1 site is also discovered in $CoFe_3O_5$. The M1 site is found to have a higher BVS than M2 in other MFe_3O_5 materials and a complete Fe^{3+}/Fe^{2+} charge ordering over M1/M2 sites is observed in one phase of $CaFe_3O_5$.[10] Hence the tendency for cobalt to substitute as Co^{2+} rather than Co^{3+} probably drives the M2 octahedral site preference, although the disorder within our Co-deficient sample does not lead to a significant difference between the M1 and M2 site BVSs.

Temperature Evolution of Crystal Structure The thermal evolution of the crystal structure of $CoFe_3O_5$ between 5 and 400 K has been studied using high resolution PSXRD (Figure 3) and PND experiments. Rietveld fits showed that the orthorhombic *Cmcm* structure is adopted throughout this temperature range. Anisotropic thermal expansion of the lattice parameters is observed when cooled below $T_{C1} \approx 300$ K (Figure 4 and S3), with a and c contracting with decreasing temperature, whilst b expands. Another anomaly in the slope of the lattice parameters and cell volume is found at $T_{C2} \approx 100$ K. These observations show that the changes in magnetic order are coupled to the lattice leading to magnetostrictive effects.
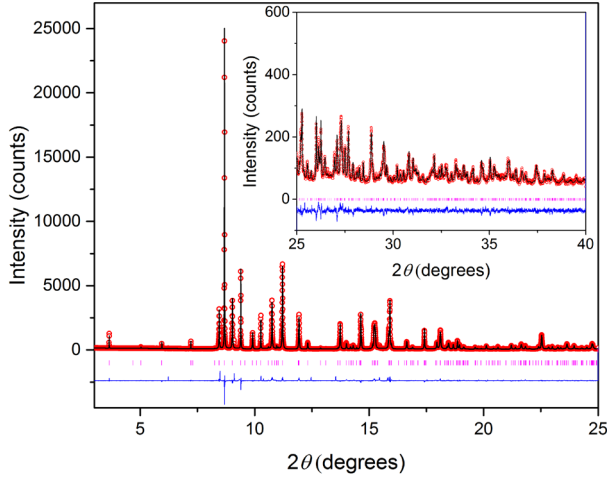
Figure 3. Rietveld fit to synchrotron powder diffraction profiles for CoFe₃O₅ at 300 K, with insert showing high angle fitting. (χ^2 = 8.5, R_{wp} = 12.3 % and R_p = 9.4 %).
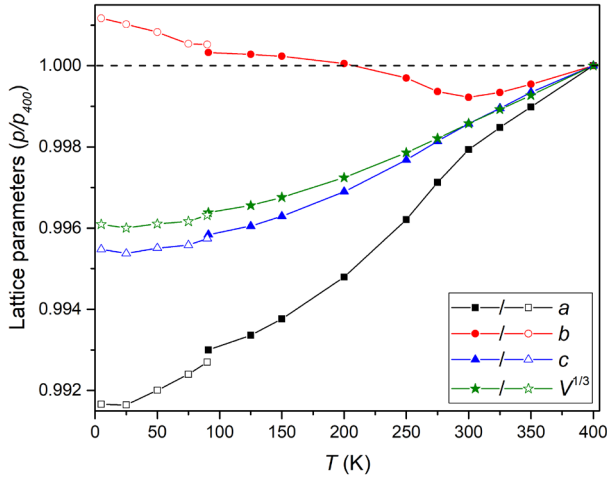

Figure 4. Changes in the lattice parameters relative to 400 K values obtained from PSXRD ($a_{400 K}$ = 2.90423(3), $b_{400 K}$ = 9.77325(8) and $c_{400 K}$ = 12.5817(1) Å). Open/closed points were collected using helium cryostat/nitrogen cryostream systems.
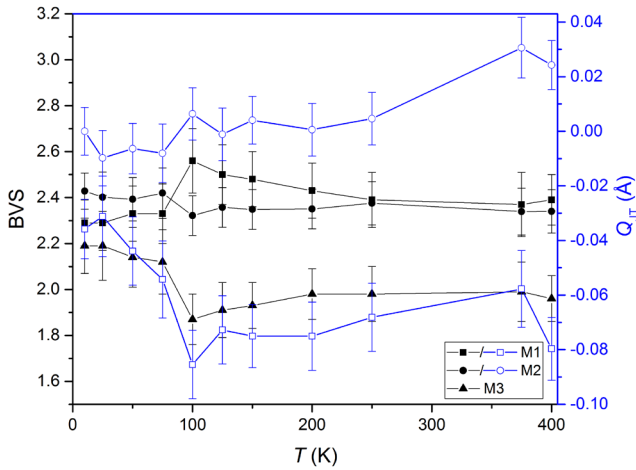

Figure 5. Temperature evolution of BVS (black points) and the tetragonal Jahn-Teller distortion parameter Q_{JT} for the octahedral cation sites in CoFe₃O₅, obtained from PND data.

Refined coordinates do not reveal any large changes in the crystal structure between 10 and 400 K. BVS's shown in Figure 5 remain approximately constant on cooling although slight anomalies are seen around $T_{C2} \approx 100$ K accompanied by an increase in the tetragonal Jahn-Teller distortion parameter Q_{JT} at site M1. The latter is consistent with intersite charge transfer increasing the Fe^{3+}/Fe^{2+} ratio, as Fe^{3+} has intrinsic Q_{JT} = 0 while orbitally-degenerate Fe^{2+} has negative Q_{JT}. Hence there are traces of the charge ordering seen in other MFe₃O₅ materials, but the cation disorder in CoFe₃O₅ suppresses any clear charge and orbital ordering.

Magnetic Structures High resolution PND patterns collected at 10, 50, 150 and 400 K and additional short scans at intermediate temperatures were used to determine the magnetic structures of CoFe₃O₅ and to study their thermal evolution. Plots in Figure 6a reveal the appearance of magnetic reflections when CoFe₃O₅ is cooled below $T_{C1} \approx 300$ K and additional magnetic peaks are observed below $T_{C2} \approx 100$ K. All of the magnetic reflections in both regimes were indexed by propagation vector [0 0 0], and analysis of the resulting irreducible representations for the spin order is shown in Table S2 with refined moment components in Table S3. The refined magnetic structures gave good fits to the data as shown in Figure 6b. The magnetic contribution of the rock salt Co₀.₈₆Fe₀.₁₄O phase, where spins order antiferromagnetically below ~300 K with a propagation vector of [½ ½ ½], was also included in the refinements.

The magnetic structures adopted by CoFe₃O₅ below T_{C1} and T_{C2} are presented in Figures 7a and 7b, respectively, and the thermal evolutions of the ordered moments are shown in Fig 7c. On cooling below $T_{C1} \approx 300$ K, the spins at the octahedral M1 and M2 sites order antiferromagnetically parallel to the c axis, whilst the M3 spins remains disordered. Canting of the spins towards the b-axis is allowed by symmetry although the ordered component is too small to refine, and this weak ferromagnetism is the likely cause of the small net magnetization observed at 200 K in Figure 2a. The additional magnetic reflections below $T_{C2} \approx 100$ K are fitted by a ferromagnetic order of the M3 spins along the a-axis with canting of the M1 spins so that they gain a ferromagnetic x-component antiparallel to the M3 spins. Further low temperature spin reorientations reported in Fe₄O₅ and MnFe₃O₅ are driven by Fe^{2+}/Fe^{3+} charge ordering. However, cation disorder in CoFe₃O₅ suppresses any charge ordering and hence no further spin canting is observed at lower temperatures. The total ordered M1 moment at 10 K of 4.3 μ_B is consistent with near-Fe^{3+} spins while smaller M2 and M3 moments of 3.3 and 2.6 μ_B reflect the Fe/Co disorder. The predicted net ferrimagnetic moment of 1.1 μ_B per formula unit at 10 K is comparable to the remnant magnetization of 0.75 μ_B observed at 2 K (Figure 2a).

The antiferromagnetic spin ordering of CoFe₃O₅ formed below T_{C1} is the same as those reported in MnFe₃O₅ and in the charge averaged phase of CaFe₃O₅.[10,12] This is favoured by dominant antiferromagnetic M1-M2 interactions through direct exchange and M-O-M superexchange between edge and corner sharing M1O₆ and M2O₆ octahedra. Weaker antisymmetric Dzyaloshinskii-Moriya (DM) interactions lead to canting and the observed weak ferromagnetism. Spins at the trigonal prismatic M3 sites are coupled to equal numbers of antiparallel M1 and M2 moments through M-O-M bridges and so their long range order is frustrated. Weaker DM interactions thus result

in ferromagnetic order of M3 moments, perpendicular to the antiferromagnetic spins, below T_{C2}. Symmetric superexchange interactions between M3 and M1 spins lead to a canting of the latter such that they gain ferromagnetic components aligned antiparallel to the M3 spins. A similar coupled order of M3 and antiparallel M1 spin components is observed in the intermediate temperature spin structure of MnFe$_3$O$_5$,[12] but with spins in the b-direction whereas those for CoFe$_3$O$_5$ are in the a-direction. The strong electronic anisotropy of Co^{2+} is likely to be responsible for the latter difference.
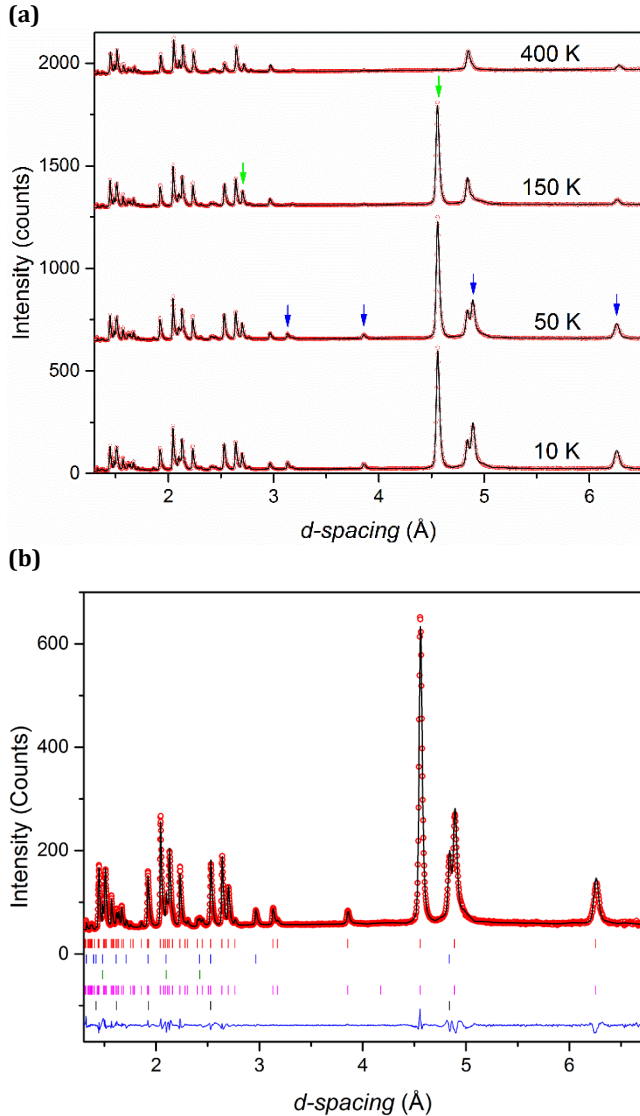
(a)

(b)

Figure 6. (a) Temperature evolution of the neutron diffraction pattern of CoFe$_3$O$_5$. Magnetic peak contributions indicated by green arrows in the 150 K pattern are (021) and (111), and those indicated by blue arrows at 50 K are (002), (020), (022) and (004), in order of descending d-spacing. Rietveld fits to the profiles are shown. (b) Full Rietveld plot for the 10 K data. Markers from top to bottom respectively show reflections from nuclear CoFe$_3$O$_5$, CoFe$_2$O$_4$ and CoO, and magnetic CoFe$_3$O$_5$ and CoO type phases. (χ^2 = 12.5, R_{wp} = 9.2% and R_p = 10.1%).

Conclusion

The above results demonstrate that the series of orthorhombic Sr$_2$Tl$_2$O$_5$-type MFe$_3$O$_5$ ferrites can be extended to M = Co, although a Co-deficient Co$_{0.6}$Fe$_{3.4}$O$_5$ phase was obtained from synthesis at 12 GPa suggesting that higher pressures may be required to stabilize the ideal stoichiometry.

(a)
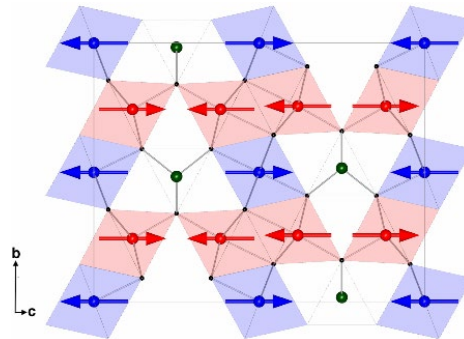
(b)
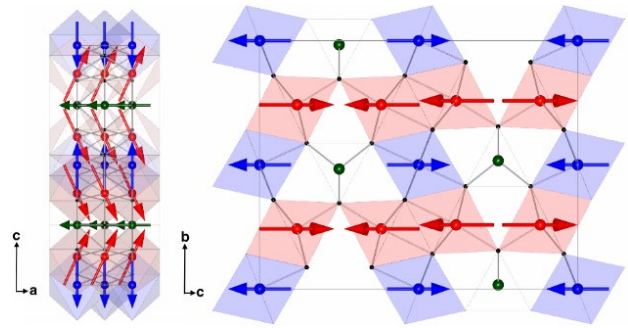
(c)
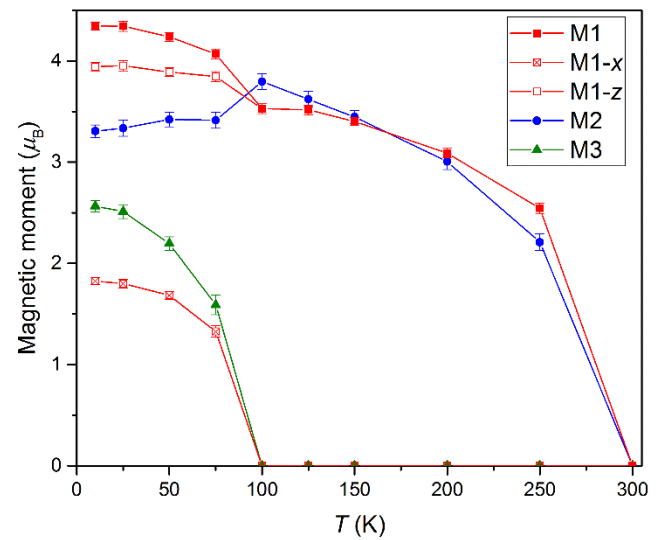
Figure 7. Magnetic structures of CoFe$_3$O$_5$ at (a) 150 and (b) 10 K. Octahedral M1 and M2 and trigonal prismatic M3 sites and moments are shown as red, blue and green, respectively. (c) The temperature evolution of the ordered magnetic moments and the x and z components for the M1 spins.

The cation distribution determined from neutron diffraction is found to be profoundly different from those in previously

5

studied MFe_3O_5 derivatives of Fe_4O_5. Materials with M^{2+} = Ca and Mn cations larger than Fe^{2+} adopt normal cation distributions with M^{2+} only at the trigonal prismatic sites. The present study shows that Co^{2+} substitutes more evenly across trigonal prismatic and octahedral sites, so the cation distribution lies between normal and inverse MFe_3O_5 limits. A surprisingly strong preference for Co to substitute at just one of the two octahedral sites is also revealed. This likely reflects differing site potentials although the disorder within our sample does not lead to a significant difference between octahedral site bond valence sums.

$CoFe_3O_5$ shows complex magnetic behavior with weak ferromagnetism (canted antiferromagnetism) below $T_{C1} \approx 300$ K and a second transition to ferrimagnetic order at $T_{C2} \approx 100$ K. Spin scattering of carriers leads a substantial increase in the hopping activation energy below T_{C1} and a small negative magnetoresistance is observed at low temperatures.

ASSOCIATED CONTENT

Supporting Information.
Supporting Information is available free of charge via the Internet at http://pubs.acs.org.
Data that support the findings of this study have been deposited at https://datashare.is.ed.ac.uk/handle/10283/838.

AUTHOR INFORMATION

Corresponding Author
E-mail: j.p.attfield@ed.ac.uk

ORCID
Ka H. Hong: 0000-0002-6894-6711
Elena Solana-Madruga: 0000-0001-6175-6053
Mauro Coduri: 0000-0002-5387-8947
J. Paul Attfield: 0000-0001-9763-3987

Author Contributions
The manuscript was written through contributions of all authors.

REFERENCES

(1) Verwey, E. J. W. Electronic conduction of magnetite (Fe3O4) and its transition point at low temperatures. *Nature* **1939**, *144*, 327–328.

(2) Senn, M. S.; Wright, J. P.; Attfield, J. P. Charge order and three-site distortions in the Verwey structure of magnetite. *Nature* **2012**, *481*, 173–176.

(3) Lavina, B.; Dera, P.; Kim, E.; Meng, Y.; Downs, R. T.; Weck, P. F.; Sutton, S. R.; Zhao, Y. Discovery of the recoverable high-pressure iron oxide Fe4O5. *Proc. Natl. Acad. Sci. U. S. A.* **2011**, *108*, 17281–5.

(4) Ovsyannikov, S. V.; Bykov, M.; Bykova, E.; Kozlenko, D. P.; Tsirlin, A. A.; Karkin, A. E.; Shchennikov, V. V.; Kichanov, S. E.; Gou, H.; Abakumov, A. M.; Egoavil, R.; Verbeeck, J.; McCammon, C.; Dyadkin, V.; Chernyshov, D.; van Smaalen, S.; Dubrovinsky, L. S. Charge-ordering transition in iron oxide Fe4O5 involving competing dimer and trimer formation. *Nat. Chem.* **2016**, 1–8. doi:10.1038/nchem.2478

(5) Lavina, B.; Meng, Y. Unraveling the complexity of iron oxides at high pressure and temperature: Synthesis of Fe5O6. *Sci. Adv.* **2015**, *1*, e1400260.

(6) Delacotte, C.; Hüe, F.; Bréard, Y.; Hébert, S.; Pérez, O.; Caignaert, V.; Greneche, J. M. and Pelloquin, D. Structural Transition at 360 K in the CaFe5O7 Ferrite: Toward a New Charge Ordering Distribution. *Inorg. Chem.*, **2014**, *53*, 10171–10177.

(7) Delacotte, C.; Bréard, Y.; Caignaert, V.; Hardy, V.; Greneche, J. M.; Hébert, S.; Suard E.; Pelloquin, D. Transmission Electron Microscopy Study of CaFe5O7 : Evidence of a Monoclinic Superstructure at Room Temperature. *Key Eng.Mater.* **2014**, *617,* 237–240.

(8) Delacotte, C.; Bréard, Y.; Caignaert, V.; Hardy, V.; Greneche, J. M.; Hébert, S.; Suard E.; Pelloquin, D. Morin-like spin canting in the magnetic CaFe5O7 ferrite: A combined neutron and Mössbauer study. *J. Solid State Chem.* **2017**, *247*, 13–19.

(9) Evrard, O.; Malaman, B.; Jeannot, F. Mise en évidence de CaFe4O6 et détermination des structures cristallines des ferrites de calcium CaFe2+*n*O4+*n* (*n* =1, 2, 3): nouvel exemple d'intercroissanc. *J. Solid State Chem.* **1980**, *35*, 112–119.

(10) Hong, K. H.; Arevalo-Lopez, A. M.; Cumby, J.; Ritter, C.; Attfield, J. P. Long range electronic phase separation in CaFe3O5. *Nat. Commun.* **2018,** DOI: 10.1038/s41467-018-05363-6.

(11) Hong, K. H.; McNally, G. M.; Coduri, M.; Attfield, J. P. Synthesis, crystal structure, and magnetic properties of MnFe3O5. *Zeitschrift für Anorg. und Allg. Chemie* **2016**, *642*, 1355–1358.

(12) Hong, K. H.; Arevalo-Lopez, A. M.; Coduri, M.; McNally, G. M.; Attfield, J. P. Cation, magnetic, and charge ordering in MnFe3O5. *J. Mater. Chem. C* **2018**, *6,* 3271–3275.

(13) Uenver, L.; Woodland, A. B.; Miyajima, N.; Ballaran, T. B.; Frost, D. J. Behaviour of Fe4O5–Mg2Fe2O5 solid solutions and their relation to coexisting Mg–Fe silicates and oxide phases. *Contrib. to Mineral. Petrol.* **2018**, *173,* 1–16.

(14) Berastegui, P.; Eriksson, S.; Hull, S.; García García, F. J.; Eriksen, J. Synthesis and crystal structure of the alkaline-earth thallates MnTl2O3+n (M = Ca, Sr). *Solid State Sci.* **2004**, *6*, 433–441.

(15) Rodriguez-Carvajal, J. Recent advances in magnetic structure determination by neutron powder diffraction. *Phys. B.* **1993,** *192,* 55-69.

(16) Larson, A. C.; Von Dreele, R. B. General Structure Analysis System (GSAS). *Los. Alamos National Laboratory Report LAUR,* **2004,** *748,* 86–748.

(17) Momma, K.; Izumi, F. VESTA 3 for three-dimensional visualization of crystal, volumetric and morphology data. *J. Appl. Crystallogr.*, **2011,** *44,* 1272–1276.

(18) Attfield, J. P. Charge ordering in transition metal oxides. *Solid State Sci.* **2006**, *8*, 861–867.

(19) Brown, I. D. VALENCE: a program for calculating bond valences. *J. Appl. Crystallogr.* **1996**, 479–480 doi:10.1107/S002188989600163X

SYNOPSIS TOC The ferrite $CoFe_3O_5$ prepared at high pressure has Co^{2+} substituted across trigonal prismatic and octahedral sites leading to complex magnetic behavior with weak ferromagnetism below $T_{C1} \approx 300$ K and a second transition to the canted ferrimagnetic order shown below at $T_{C2} \approx 100$ K.